Nanoscale chemical analysis and imaging of solid oxide cells

Hauch, Anne; Bowen, Jacob R.; Kuhn, Luise Theil; Mogensen, Mogens Bjerg

Published in:
Electrochemical and Solid-State Letters

Link to article, DOI:
10.1149/1.2828845

Publication date:
2008

Document Version
Publisher's PDF, also known as Version of record

Electrochemical and Solid-State Letters, **11** (3) B38-B41 (2008)
1099-0062/2008/11(3)/B38/4/$23.00 © The Electrochemical Society

Nanoscale Chemical Analysis and Imaging of Solid Oxide Cells

Anne Hauch,[z] Jacob Ross Bowen, Luise Theil Kuhn, and Mogens Mogensen*

Fuel Cells and Solid State Chemistry Department, Risø National Laboratory, Technical University of Denmark, DK-4000 Roskilde, Denmark

The performance of solid oxide cells (SOCs) is highly dependent on triple phase boundaries (TPBs). Therefore, detailed TPB characterization is crucial for their further development. We demonstrate that it is possible to prepare a ~50 nm thick transmission electron microscopy (TEM) lamella of the interface between the dense ceramic electrolyte and the porous metallic/ceramic hydrogen electrode of an SOC using focused ion beam milling. We show combined TEM/scanning TEM/energy-dispersive spectroscopy investigations of the nanostructure at the TPBs in a high-performance SOC. The chemical composition of nanoscale impurity phases at the TPBs has been obtained with a few nanometers lateral resolution.
 [DOI: 10.1149/1.2828845]

Manuscript submitted September 26, 2007; revised manuscript received December 5, 2007.
Available electronically January 7, 2008.

Solid oxide cells (SOCs) can be operated as solid oxide fuel cells (SOFCs) to produce electrical energy and as solid oxide electrolysis cells (SOECs) to produce fuels such as H_2 or synthesis gas (H_2 + CO). For SOCs to become a commercially mature technology, it is necessary to produce low-cost cells with high reproducibility, high performance, and long-term stability. A key parameter for the performance of SOCs is the triple phase boundary (TPB) in the electrodes where the electrochemical reactions occur. A schematic illustration of a catalytically active TPB available for the electrochemical reaction in the H_2 electrode of an SOFC using conventional materials such as Ni and yttria-stabilized zirconia (YSZ) is shown to the left in Fig. 1, and a catalytically inactive TPB blocked by an impurity phase is shown to the right. A simplified scheme for the reaction in an SOC hydrogen electrode is

$$H_2(\text{gas,pores}) + O^{2-}(\text{YSZ}) \underset{\text{SOEC}}{\overset{\text{SOFC}}{\rightleftarrows}} 2e^-(\text{Ni}) + H_2O(\text{gas,pores}) \quad [1]$$

An increase in the density of blocked TPBs in an electrode structure leads to an increase in the resistance of the cell and therefore a decrease in the cell performance.

Studies of model systems and half cells have shown that the degree of impurities in the raw materials greatly influences the performance of a cell and the degree of passivation. Impurities tend to agglomerate at the TPBs, and their thickness need only be a few nanometers to significantly decrease cell performance.[1-4] Therefore, a detailed high-resolution characterization of the interfacial structure and chemical analysis of the TPB in the SOC electrodes is necessary to understand the observed performance loss of SOCs. For this purpose, a combined transmission electron microscopy (TEM)/scanning TEM (STEM)/energy-dispersive spectroscopy (EDS) analysis is advantageous. Initial results on quantification of the TPB in an SOFC H_2 electrode was reported by Wilson et al.,[5] and others have reported on the effect of the TPBs in the electrode nanostructure on the performance of the cell.[6] Previously only a few TEM studies of the electrodes of full and half cells have been reported,[7-9] and interface TEM studies have been particularly limited due to difficulties in specimen preparation. In this work we report a nanoscale chemical analysis and imaging of impurities segregated at the TPBs in the H_2 electrode of a degraded SOC.

Experimental

The cell used for testing prior to the electron microscopy characterization was a Ni/YSZ supported DK-SOFC cell produced at Risø National Laboratory, Denmark.[10,11] The cell had a 10–15 μm thick hydrogen electrode of Ni/YSZ cermet, a 10–15 μm thick YSZ electrolyte, and a 15–20 μm thick strontium-doped lanthanum manganite (LSM)–YSZ composite oxygen electrode, and was supported by a ~300 μm thick Ni/YSZ layer. The ratio between Ni and YSZ (TZ8Y, Tosoh Corporation, ZrO_2 stabilized with 8 mol % Y_2O_3) was 40/60 vol %. The composition of the LSM was $(La_{0.75}Sr_{0.25})_{0.95}MnO_3$, and the LSM/YSZ ratio in the composite oxygen electrode was 50/50 vol %. Cell-test setup and initial cell characterization is described elsewhere.[12,13]

Field-emission gun (FEG) scanning electron microscopy (SEM) imaging and Ga^+ focused ion beam (FIB) milling (30 keV) was performed on a Zeiss Crossbeam 1540XB. Platinum was used as the protective layer on the sample surface prior to FIB milling, and tungsten was deposited to attach the lamella to the TEM Cu Omniprobe holder prior to final polishing.

A JEM-3000F FEG-TEM equipped with a Gatan imaging filter and an option for STEM was used to perform TEM, STEM, and electron energy loss spectroscopy (EELS) analysis. In STEM mode a high angular annular dark-field (HAADF) detector was used and the beam diameter was 0.2 nm. The energy-dispersive X-ray microanalysis system Oxford Instruments INCA was used to perform EDS. All spectra were acquired with an acquisition time of 60 s, and the EDS map in Fig. 5 was acquired in 30 min. Quantification of EDS was performed by standardless analysis using the Cliff–Lorimer correction with absorbance in the Thermo Fisher NoranSystemSix software version 1.5.

Results and Discussion

To obtain nanoscale chemical characterization of the TPBs we have combined FIB milling and FEG-SEM with analytical TEM, STEM, and EDS. Using FIB/FEG-SEM is advantageous as it allows TEM specimen preparation from site-specific locations with submicrometer precision. Furthermore, the heterogeneous and highly porous electrode structure can be uniformly thinned.

The hydrogen-electrode-supported SOC for the TEM/STEM/EDS study presented here was similar to cells that have previously shown excellent initial performance.[12,13] The SOC was subjected to a galvanostatic 1300 h electrolysis test [850°C, −0.5 A/cm^2, gas mixture of $p(H_2)/p(H_2O) = 0.5/0.5$ at the hydrogen electrode]. The

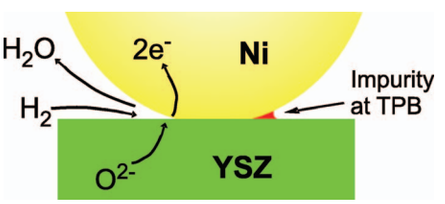

Figure 1. A schematic illustration of TPBs in an SOC H_2 electrode: (left) a TPB accessible for the electrochemical reaction and (right) a TPB blocked by an impurity phase. A typical diameter for the Ni particles is ~1 μm.

* Electrochemical Society Active Member.
[z] E-mail: anne.hauch@risoe.dk

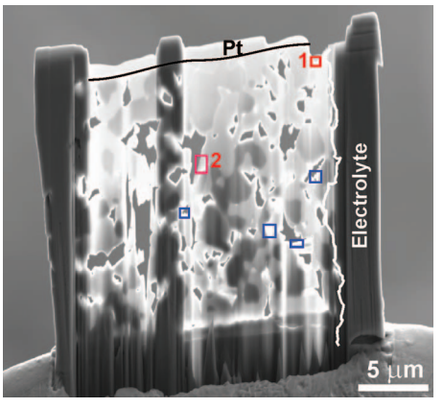

Figure 2. SEM micrograph of the TEM lamella obtained by FIB milling and lift-out technique for the H_2 electrode/electrolyte interface. TEM and STEM micrographs of the region marked by the red square (1) are shown in Fig. 3. EDS mapping of the region marked by the red rectangle (2) is shown in Fig. 5. The blue rectangles mark regions where further impurity phases were analyzed.

cell-test results showed a decrease in the performance of the cell of 2% per 1000 h, caused largely by an increase in polarization resistance related to processes in the hydrogen electrode.[13] Therefore, a systematic post-test investigation of the interface between the porous (~30%) Ni/YSZ hydrogen electrode and the YSZ electrolyte was performed.

First, a cell fragment with an H_2 electrode/electrolyte interface length of ~1 cm was investigated by FEG-SEM to confirm that the electrode nanostructure of the interface was representative over larger regions. Second, X-ray spectra were obtained in different regions of the interface in order to select a representative interfacial area for FIB milling containing at least one impurity phase in the polished cross section. An interfacial region with an impurity phase adjacent to the electrolyte was located and a 3 μm thick protective layer of platinum was deposited on the area of interest. The in situ lift-out technique[14] was used to create and transfer the ~500 nm thick sample from the bulk of the SOC and attach it to a TEM holder for final thinning. Even though the H_2 electrode is highly porous and consists of materials of different hardness (Ni and YSZ), it was possible to thin a lamella of homogeneous thickness suitable for TEM investigations. Figure 2 shows the lamella after final polishing prior to TEM investigation. The black line in Fig. 2 indicates the border between the protective Pt layer and the electrode. The lamella has an electrode/electrolyte interface length of ~17 μm. An area of ~275 μm^2 was thinned in the electrode until significant 10 keV electron transparency in the SEM was obtained (Fig. 2), providing a lamella with numerous TPBs. For stability reasons, the final milling was omitted for a ~2 μm bar of material parallel to the electrode/electrolyte interface in the center of the electrode. The thickness of the lamella was measured to be ~50 nm in the thinned regions by imaging using FE-SEM and confirmed by EELS using TEM in the region with the impurity phase marked by the blue square closest to the electrolyte in Fig. 2. TEM imaging of the lamella indicated thickness variations across the lamella; nevertheless, it contained several regions suitable for high-resolution TEM where lattice fringes could be observed in the Ni and YSZ particles.

Impurities containing oxides of Si, Al, and occasionally Na were observed at six different locations in the lamella which are marked by the rectangles in Fig. 2. All impurity phases were found at locations in the electrode nanostructure that were TPBs prior to the contamination with impurities.

A typical example of a Si and Al oxide containing impurity phase at a TPB is shown in the bright-field TEM micrograph in Fig. 3a, and its position in the lamella is shown by the red square marked 1 in Fig. 2. The alumina phase in Fig. 3a most likely originates from

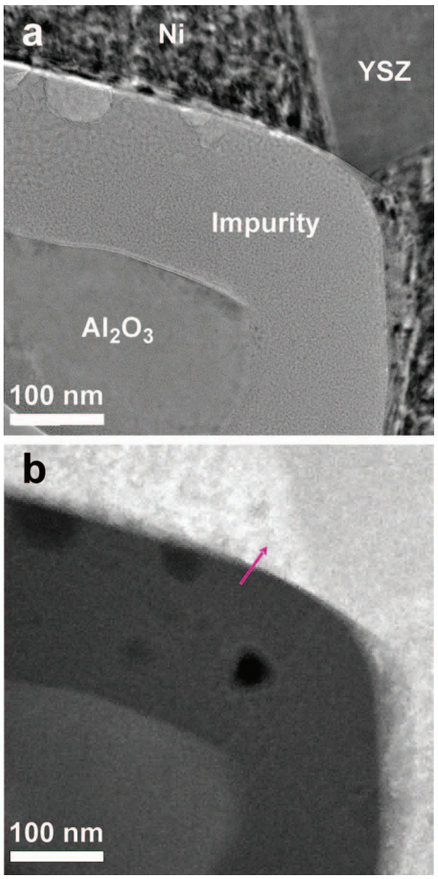

Figure 3. (a) Bright-field TEM micrograph and (b) HAADF STEM micrograph of the impurity marked by the red square (1) in Fig. 2. The arrow marks the position for the line scan, from which results are given in Fig. 4.

the addition of Al_2O_3 as sintering aid during production of the cells. The glassy impurity phase surrounding the alumina particle is spread out along the original TPB. In this impurity phase FIB artifacts in the form of redeposited Ni were observed as crystalline particles with a diameter of a few nanometers.[13] This was confirmed by nanobeam EDS in STEM mode on these particles and also in the impurity phase next to them. Spectra obtained on the crystalline particles showed a significant enrichment of Ni. A maximum of three metal atom percent of Ga from the FIB preparation was detected in the lamella.

An STEM micrograph using an HAADF detector of the same area as the TEM micrograph in Fig. 3a is shown in Fig. 3b. STEM mode has the following advantages when investigating the TPB in the hydrogen electrode: (*i*) the atomic number contrast obtained using the HAADF detector facilitates the discrimination of the light element impurity phases and thin films of redeposited material from the Ni and YSZ particles directly, (*ii*) the STEM beam is less harmful than a convergent TEM beam to the sample, e.g., when recording EDS, and (*iii*) the beam diameter is only 0.2 nm, thus providing a high lateral EDS resolution in STEM mode. The beam damage effect of recording EDS in TEM mode using a focused electron beam is seen in Fig. 3b as a black spot, i.e., hole, in the impurity phase. In STEM mode EDS was obtained for selected areas of the impurity phase and the Al/Si ratio was found to be 35/44 with a relative uncertainty of ~10%.

The arrow in Fig. 3b marks the position for the EDS line scan, from which results are shown in Fig. 4. This line scan was performed in STEM mode with a beam diameter of 0.2 nm. The thickness of the lamella in this region is estimated to be ~50 nm by

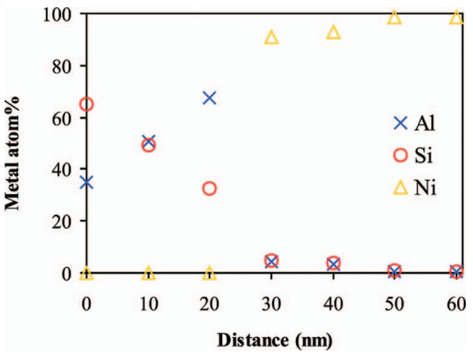

Figure 4. Metal atom percentages of Ni, Al, and Si over the interface marked by the arrow in Fig. 3b. The relative uncertainty for the metal atom percentages is ~10%. The applied beam diameter was 0.2 nm. Cu and redeposited Ni has been omitted in the calculations (see details in the text).

EELS. Using an average density of ~3 g/cm^3 for this phase, a beam spread of ~1 nm was estimated.[15] The EDS data obtained in STEM mode for this sample can therefore provide chemical compositions of the imaged impurities with a subnanometer lateral resolution. The EDS points in the line scan in Fig. 4 were obtained with a pitch of 10 nm (50 × beam diameter), therefore yielding no overlap in the interaction volume for each point. However, under the given experimental conditions, the chemical composition of the impurity/Ni interface could easily have been resolved with a pitch of 1–2 nm. From the line-scan results it is observed that the Si and Al oxide impurity phase is delineated by a distinct phase boundary without a diffusion gradient into the Ni particle. This was further confirmed by EDS in a selected area marked "Ni" in Fig. 3a. In this area, the only element detected was Ni (and background Cu). In Fig. 4 the Ni content due to redeposited Ni has been subtracted for the three spectra recorded in the impurity phase. The net count for the Ni_K peak was 282 ± 31 for a point spectrum in STEM mode recorded on one of the crystalline particles of redeposited Ni on the impurity phase. None of the spectra recorded in the impurity phase during the line scan had a Ni_K net count above this. As this Ni contribution is an FIB artifact, it has been corrected for in Fig. 4.

From Fig. 4 it is also observed that the chemical composition, as evident from the Al/Si ratio, of the impurity phase varies greatly over a 30 nm range. This difference in the Al/Si ratio has also been observed in the other impurity phases in this lamella. Based upon the observed "nanoheterogeneity" of the impurity phase, it is assumed that nanocrystalline particles exist in the amorphous glassy phase impurity.

Besides impurities of Si and Al oxides, three of the six detected impurities in this TEM lamella also contained Na. One of these Na-containing impurities at a TPB is shown by the EDS map given in Fig. 5 with the HAADF STEM micrograph of the same area. The chemical composition of the silicon-containing impurity phase in Fig. 5 was found to have an atom ratio of Na/Al/Si ~ 1/3/3, which is representative of the three Na-containing impurity phases observed in this TEM lamella.

Furthermore, Fig. 5 illustrates how a site that, presumably, was originally a TPB (marked by the arrow in Fig. 5) is now completely blocked by an impurity phase. The impurity phase appears to have begun building up at the exact position of the TPB and grown outward to cover several hundred nanometers in the vicinity of the TPB, and thereby hampering the electrochemical reaction (Eq. 1). The findings of impurities confirm the results from electrochemical impedance spectroscopy characterization of this cell during testing.[13]

Conclusion

We have shown that by combining the following three techniques, (*i*) in situ site specific FIB preparation of large-area TEM lamella of the electrode/electrolyte interface, (*ii*) TEM/STEM imaging of the TPBs, and (*iii*) EDS for nanoscale chemical analysis of impurities and interfaces, we were able to obtain detailed information on the impurity phases accumulated at the TPBs of an SOC H_2 electrode/electrolyte interface. Regarding both the lateral resolution of the analysis of the chemical composition and the structure, the information is obtained on the nanometer scale. Six impurity phases were found in the 275 μm^2 electrode area of the lamella. They all contained Al and Si oxides, and three of them also contained sodium oxide. The ratio of Na/Al/Si was ~1/3/3.

The present work illustrates that Si-containing impurities can build up in the H_2 electrode nanostructure at the TPBs and hamper the electrochemical reactions for initially high-performing SOCs during long-term operation. FIB/TEM/STEM/EDS investigations presented here of the TPBs of SOC electrodes are a key method for understanding impurities and their effects on performance of SOCs and are thus a critical step in the development of high-performing and long-term stable SOCs.

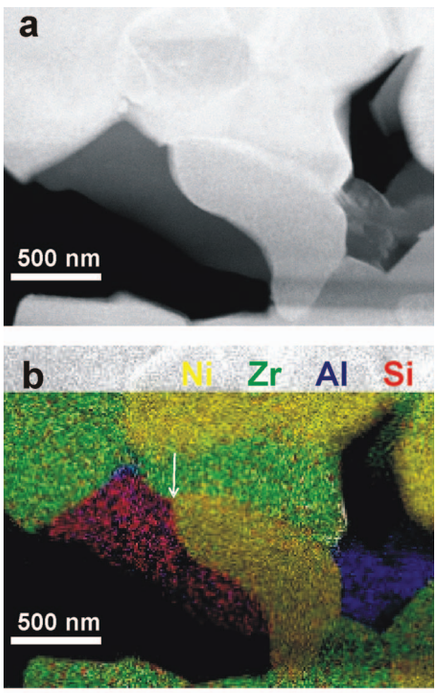

Element	Na	Al	Si	Ni	Cu	Zr
Metal atom%	13±2	36±2	41±3	2±1	7±1	1±1

Figure 5. (a) A HAADF STEM micrograph and (b) an EDS map of alumina-silicate impurity at a TPB. The area for this EDS map is marked by the red rectangle marked 2 in Fig. 2. The arrow marks the TPB. The impurity phase is a Na-containing alumina-silicate. Na is not visible in the map when both the Si and Al maps are overlaid; however Na is solely located within the alumina-silicate phase. Average metal atom percentages for the alumina-silicate impurity phase are given below the EDS map. Dark regions are porosities.

Acknowledgments

The authors gratefully acknowledge Dr. J. Wagner (Lund University, Faculty of Engineering) for TEM assistance. This work was supported by the European Commission via the project "Hi2H2," contract no. FP6-503765, and Energinet.dk via project PSO2007-1-7124.

Risø National Laboratory, Technical University of Denmark assisted in meeting the publication costs of this article.

References

1. K. V. Jensen, R. Wallenberg, I. Chorkendorff, and M. Mogensen, *Solid State Ionics*, **160**, 27 (2003).
2. Y.-L. Liu and C. Jiao, *Solid State Ionics*, **176**, 435 (2005).
3. K. V. Jensen, K. Norrman, and M. Mogensen, *J. Electrochem. Soc.*, **151**, 1436 (2004).
4. S. P. S. Badwal, *Solid State Ionics*, **76**, 67 (1995).
5. J. R. Wilson, W. Kobsiriphat, R. Mendoza, H.-Y. Chen, J. M. Miller, D. J. Miller, K. Thornton, P. W. Voorhees, S. B. Adler, and S. A. Barnett, *Nat. Mater.*, **5**, 541 (2006).
6. M. J. L. Østergard, C. Clausen, C. Bagger, and M. Mogensen, *Electrochim. Acta*, **40**, 1971 (1995).
7. T. Z. Sholklapper, V. Radmilovic, C. P. Jacobson, S. J. Visco, and L. C. De Jonghe, *Electrochem. Solid-State Lett.*, **10**, B74 (2007).
8. P. Piccardo, S. Chevalier, R. Molins, M. Viviani, G. Caboche, G. A. Barbucci, M. Sennour, and R. Amendola, *Surf. Coat. Technol.*, **201**, 4471 (2006).
9. S. Suzuki, H. Uchida, and M. Watanabe, *Solid State Ionics*, **177**, 359 (2006).
10. A. Hagen, R. Barfod, P. V. Hendriksen, Y.-L. Lin, and S. Ramousse, *J. Electrochem. Soc.*, **153**, A1165 (2006).
11. P. H. Larsen, C. Bagger, S. Linderoth, M. Mogensen, S. Primdahl, M. J. Jørgensen, P. V. Hendriksen, B. Kindl, N. Bonanos, F. W. Poulsen et al., in *SOFC VII*, H. Yokokawa and S. C. Singhal, editors, PV 2001-16, p. 28, The Electrochemical Society Proceedings Series, Pennington, NJ (2001).
12. A. Hauch, S. H. Jensen, M. Mogensen, and S. Ramousse, *J. Electrochem. Soc.*, **153**, A1741 (2006).
13. A. Hauch, Ph.D. Thesis, Risø National Laboratory, Technical University of Denmark, Roskilde, Denmark (2007).
14. L. A. Giannuzzi and F. A. E. Stevie, *Introduction to Focused Ion Beams. Instrumentation, Theory, Techniques and Practice*, Springer, New York (2005).
15. P. J. Goodhew, J. Humphrey, and R. Beanland, *Electron Microscopy and Analysis*, Taylor and Francis, London (2001).